Annealing-environment effects on the properties of CoPt nanoparticles formed in single-crystal Al_2O_3 by ion implantation

C. W. White,[a] S. P. Withrow, J. D. Budai, and D. K. Thomas
Oak Ridge National Laboratory, Oak Ridge, Tennessee 37831

J. M. Williams
BronteK Delta Corporation, Radford, Virginia 24141

A. Meldrum
The University of Alberta, Edmonton, Alberta T6G 2M7, Canada

K. D. Sorge
The University of Tennessee, Knoxville, Tennessee 37996

J. R. Thompson
Oak Ridge National Laboratory, Oak Ridge, Tennessee 37831 and The University of Tennessee, Knoxville, Tennessee 37996-1200

G. W. Ownby, J. F. Wendelken, and L. A. Boatner
Oak Ridge National Laboratory, Oak Ridge, Tennessee 37831

(Received 27 July 2005; accepted 24 October 2005; published online 9 December 2005)

The ion implantation of nearly equal doses of Co and Pt into a single-crystal Al_2O_3 host followed by thermal annealing leads to the formation of nanoparticles whose phase, structure, and physical properties are strongly dependent on the annealing environment. Annealing in 96% Ar+4% H_2 gives rise to ferromagnetic, chemically ordered CoPt nanoparticles with the $L1_0$ structure and a magnetic coercivity that can exceed 10 kOe at 5 K. Annealing in O_2 (or in Ar) does not result in the formation of a CoPt alloy. Instead, the implanted Pt precipitates to form oriented elemental Pt nanoparticles, and the implanted Co combines with oxygen to form Co_3O_4 oxide nanoparticles. Annealing in ultrahigh-vacuum conditions results in a mixture of phases including $CoPt_3$ and Co_3O_4 and possibly Co. The results obtained for Co+Pt-implanted Al_2O_3 are compared with the previous results for Fe+Pt-implanted Al_2O_3 annealed in similar environments. © *2005 American Institute of Physics*.
[DOI: 10.1063/1.2138801]

I. INTRODUCTION

CoPt and FePt alloys with the chemically ordered $L1_0$ structure have attracted considerable interest recently due to their unusual magnetic properties. In particular, as ordered alloys, these materials have a very high magnetocrystalline anisotropy and relatively large magnetization, and these properties make them interesting candidates for ultrahigh-density data storage applications.[1] Various techniques have been used previously to produce thin films or nanoparticles of these ordered alloys. These techniques include sputtering,[2–5] *e*-beam evaporation,[6] molecular-beam epitaxy,[7] chemical reduction,[8,9] microemulsion deposition,[10] and electrodeposition.[11]

Recently, we have demonstrated that encapsulated arrays of nanoparticles of CoPt (Ref. 12) and FePt (Refs. 13 and 14) with a wide range of compositions can be formed in the near-surface region of single-crystal Al_2O_3 by ion-beam synthesis. In this approach, the sequential implantation of Co (or Fe) and Pt ions is used to create overlapping profiles of the alloy constituents in the near surface of Al_2O_3. Thermal annealing in an atmosphere of 96% Ar+4% H_2 (ArH_2) leads to precipitation and the formation of crystallographically oriented, ordered alloy nanoparticles of $Co_{1-x}Pt_x$ (or $Fe_{1-x}Pt_x$) in the single-crystal Al_2O_3 matrix. The alloy composition x is controlled by the relative doses of implanted Co (or Fe) and Pt ions, and this allows the properties of the nanoparticles to be studied over a wide range of compositions. For both $Co_{1-x}Pt_x$ and $Fe_{1-x}Pt_x$ nanoparticles synthesized in this manner, we have found that the ordered, face-centered-tetragonal (fct) $L1_0$ structure is formed for alloy compositions in the range $x \sim 35\%$ to $\sim 60\%$. In this concentration range, the nanoparticles are ferromagnetic with magnetic coercivities that are strong functions of the alloy composition. Magnetic coercivities of $\sim$14 kOe for $Co_{45}Pt_{55}$ and 22 kOe for $Fe_{55}Pt_{45}$ have been achieved at 5 K in *c*-axis-oriented Al_2O_3.

In previous work, the structure and properties of nanoparticles formed by annealing Fe+Pt-implanted Al_2O_3 were shown to be strongly dependent on the annealing environment.[15] In the present work, we demonstrate that the properties of nanoparticles formed by thermal annealing of Co+Pt-implanted Al_2O_3 can also be altered dramatically by changing the annealing environment. Here the properties and structures of nanoparticles obtained by annealing Co+Pt-implanted Al_2O_3 in atmospheres of ArH_2, O_2, Ar (99.999% purity), or ultrahigh vacuum (UHV) are deter-

[a]Electronic mail: whitecw@ornl.gov

 © 2005 American Institute of Physics

Downloaded 31 Jan 2006 to 160.91.48.40. Redistribution subject to AIP license or copyright, see http://jap.aip.org/jap/copyright.jsp

mined, and the results are correlated and contrasted with those obtained by annealing Fe+Pt-implanted Al_2O_3 in similar environments.

II. EXPERIMENTAL PROCEDURE

Single-crystal substrates of *c*-axis-oriented Al_2O_3 were implanted sequentially by Co (360 keV) followed by Pt (910 keV) to give overlapping profiles of Co and Pt with a projected range of ~175 nm for each element. Most of the samples were implanted with doses of $1\times10^{17}/cm^2$ for Co and $1.17\times10^{17}/cm^2$ for Pt in order to produce an alloy with a Pt composition of 54% [=Pt dose/(Co dose+Pt dose)] assuming complete alloying of the implanted ions. Previous work[12] has established that the maximum magnetic coercivity is achieved for this alloy composition. The implantation was carried out at elevated temperature (T=550 °C for Co and 500 °C for Pt) to try to prevent the near surface of Al_2O_3 from being turned completely amorphous by implantation-induced displacement damage. Following implantation, the samples were annealed at temperatures of 1100 °C for 2 h in a hot-wall quartz tube furnace containing flowing gases of ArH_2, O_2, or Ar (99.999% purity). For anneals in the tube furnace, the tube was evacuated to a pressure of 4×10^{-6} Torr prior to flowing the desired gas. No attempt was made to further purify the flowing gas. A few samples were annealed at 1100 °C for 2 h on a heated sample holder in UHV at a pressure of $\sim3\times10^{-9}$ Torr. Following the high-temperature anneal at 1100 °C for 2 h, the samples were slowly cooled to room temperature or were given an additional anneal at 700–750 °C for time periods ranging from 2 to 120 h, followed by slow cooling to room temperature. For CoPt, the stable phase at high temperature is the disordered face-centered-cubic phase, while the ordered fct $L1_0$ phase is stable at lower temperatures. Accordingly, the temperature for the additional anneal was chosen to be well below the temperature for the order-disorder transition (~825 °C).[16,17] Other workers[18] were able to improve the ordered volume fraction and magnetic properties of CoPt films by prolonged annealing at temperatures below the ordering temperature for the bulk alloy; but in the present work, very little improvement in the structural or magnetic properties was achieved by carrying out this additional anneal. This suggests that the time required to slowly cool the sample to room temperature (several hours) was sufficient to establish the transformation to the ordered state—even in samples subjected only to the high-temperature anneal.

The samples were characterized using 2.3 MeV He^+ Rutherford backscattering (RBS) ion channeling measurements and by x-ray diffraction (Cu $K\alpha$ radiation) using a four-circle diffractometer or a powder diffractometer. Selected samples were examined by cross-section transmission electron microscopy (TEM), and the magnetic properties were determined using a superconducting quantum interference device (SQUID) magnetometer at temperatures T=5–300 K in applied magnetic fields up to ±65 kOe.

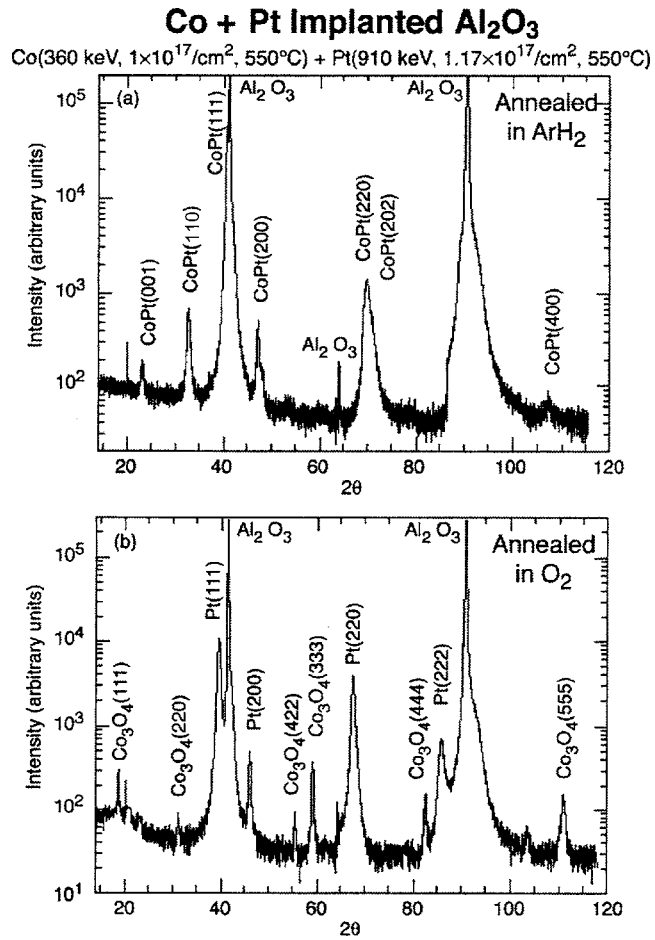

FIG. 1. X-ray-diffraction θ-2θ scans along the surface normal for *c*-axis-oriented Al_2O_3 crystals implanted by Co+Pt. The sample in (a) was annealed in flowing ArH_2 at 1100 °C/2 h+700 °C/119 h. The sample in (b) was annealed in flowing O_2 for 1100 °C/2 h+700 °C/19 h.

III. RESULTS

Figure 1 compares the x-ray-diffraction results for a sample annealed in flowing ArH_2 [Fig. 1(a)] with the results obtained from an identical sample annealed in flowing O_2 [Fig. 1(b)]. In the as-implanted state (not shown), the only diffraction lines observed are those expected from the Al_2O_3 substrate. After annealing in ArH_2 [Fig. 1(a)], the θ-2θ scans along the *c* axis of Al_2O_3 show several strong lines corresponding to those[19] of the chemically ordered (fct) $L1_0$ phase of CoPt, in addition to lines from the Al_2O_3 substrate. Consistent with our previous results,[12] the CoPt nanoparticles are oriented with respect to the *c* axis of Al_2O_3, and there are, in fact, several crystallographic orientations for the nanoparticles [i.e., CoPt (111), CoPt (110), and several other planes parallel to the Al_2O_3 (0001) planes, as shown in the spectra of Fig. 1(a)]. The CoPt (110) and CoPt (001) lines are superstructure reflections, demonstrating that at least some of the CoPt nanoparticles have the chemically ordered (fct) $L1_0$ structure, since these reflections are forbidden for the chemically disordered structure. The other lines arising from CoPt in Fig. 1(a) are fundamental reflections (allowed even in chemically disordered alloys) from fct CoPt. An order parameter S, which is a measure of the fraction of Co and Pt atoms on their ideal lattice sites, can be determined from the

Downloaded 31 Jan 2006 to 160.91.48.40. Redistribution subject to AIP license or copyright, see http://jap.aip.org/jap/copyright.jsp

ratio of integrated intensities in superstructure reflections to fundamental reflections as compared to the predicted values.[20] Using integrated intensities measured from x-ray rocking curves, the value for S is estimated to be $S \sim 0.46$ for the sample annealed in ArH_2. This value corresponds to a degree of ordering in which less than 70% of the Co and Pt atoms are located on the correct $L1_0$ lattice sites. A perfectly ordered alloy of this composition would have a value $S \sim 0.94$, and therefore the CoPt nanoparticles produced here are not fully ordered. We have not produced CoPt nanocrystal samples with $S > 0.5$ by any of the annealing sequences attempted thus far.

Figure 1(b) is the θ-2θ scan from the sample annealed in flowing O_2. In this case, there are no diffraction lines that can be identified as arising from CoPt. Instead, strong lines arising from elemental Pt [i.e., Pt (111), Pt (200), Pt (220), and Pt (222)] are observed in addition to numerous lines identified as arising from the cubic spinel, Co_3O_4 [i.e., Co_3O_4(111), Co_3O_4(220), Co_3O_4(422), Co_3O_4(333), Co_3O_4(444), and Co_3O_4(555)]. This result demonstrates that annealing in O_2 results in the precipitation of Pt and Co_3O_4 nanoparticles, with multiple crystallographic orientations of both types of nanoprecipitates. The lattice parameter determined from the Pt nanoparticles in Fig. 1(b) is $a_o = 3.92$ Å, which is the bulk Pt value. The lattice parameter determined from the reflections identified as Co_3O_4 in Fig. 1(b) is $a_o = 8.10$ Å, which is slightly expanded in comparison with that expected from pure Co_3O_4 ($a_o = 8.08$ Å). Aluminum incorporation into the Co_3O_4 nanoparticles would lead to a lattice expansion, and it is likely that some Al is incorporated into the Co_3O_4 nanoparticles.

The results illustrated in Fig. 1, therefore, demonstrate that annealing Co+Pt-implanted Al_2O_3 in flowing ArH_2 results in the formation of CoPt nanoparticles with at least some having the chemically ordered $L1_0$ structure. By contrast, annealing in flowing O_2 gives rise to the precipitation of elemental Pt nanoparticles accompanied by the formation of Co_3O_4 nanoparticles (possibly containing incorporated Al), with no evidence of CoPt formation.

Figure 2 shows the RBS channeling results in the as-implanted state and after annealing in flowing O_2. In the as-implanted state [Fig. 2(a)], the near surface of Al_2O_3 is heavily damaged and may have some regions that are nearly amorphous. Annealing in flowing O_2 gives rise to substantial recovery of the lattice damage accompanied by some redistribution of the implanted Co and, to a lesser extent, redistribution of Pt. Ion channeling is observed after annealing in both the Co and Pt parts of the spectrum, which is expected since the nanoparticles are oriented with respect to the matrix (as demonstrated by x-ray rocking curves). The Co profile after annealing has obvious structure but there is very little Co segregated to the surface (less than 4%), and there is almost no loss of implanted Co or Pt during annealing in O_2. The ion channeling results of Fig. 2(b) are quite similar to those observed previously[12] for samples annealed in ArH_2 with the exception that there is more structure in the Co profile of Fig. 2(b) than that observed after annealing in ArH_2.

The microstructure in the near surface of the sample annealed in O_2 is shown in the TEM results of Fig. 3. After annealing, a high density of voids is observed in the very near-surface region of the cross-section micrograph (Fig. 3, top). The large precipitated particles at a depth of ~200 nm have a maximum diameter of ~40 nm which is somewhat larger than the $Co_{55}Pt_{45}$ nanoparticles observed previously[12] in a sample annealed in ArH_2. In addition to the dark, nearly equiaxed particles in the cross-section micrograph, there are fainter, elongated structures observed in this micrograph. The plan-view micrograph (Fig. 3, bottom) shows the dark, nearly equiaxed particles; but in addition, there are fainter large particles which exhibit Moiré fringes. We believe that the particles that exhibit Moiré fringes in plan view are the same as those that are elongated in cross section.

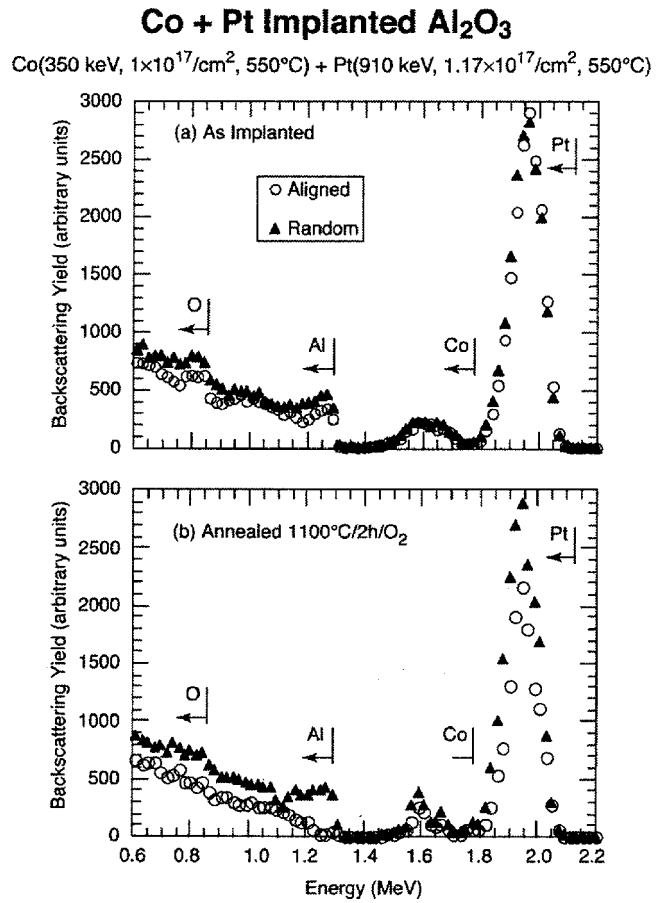

FIG. 2. RBS channeling measurements for Co+Pt-implanted Al_2O_3 in (a) the as-implanted state and (b) after annealing for 1100 °C/2 h +700 °C/19 h in flowing O_2. Spectra are shown with the He^+ beam aligned along the [0001] direction of Al_2O_3 and with the beam in a random direction. Energies for scattering from Pt, Co, Al, and O at the surface are noted.

Energy dispersive x-ray spectroscopy (EDS) measurements have been used to identify the composition of individual particles for samples annealed in O_2. The results are shown in Fig. 4. The EDS spectra from particles 1 and 4 are Pt rich. (They may be pure Pt, but lines arising from the matrix or nearby particles cannot be completely avoided.) These are the dark, nearly equiaxed particles observed in the TEM micrograph, and they are almost certainly the Pt particles identified in the diffraction results from Fig. 1(b). In addition to the particles in Fig. 4 which are Pt rich, there are also fainter elongated features in the micrograph and the

Downloaded 31 Jan 2006 to 160.91.48.40. Redistribution subject to AIP license or copyright, see http://jap.aip.org/jap/copyright.jsp

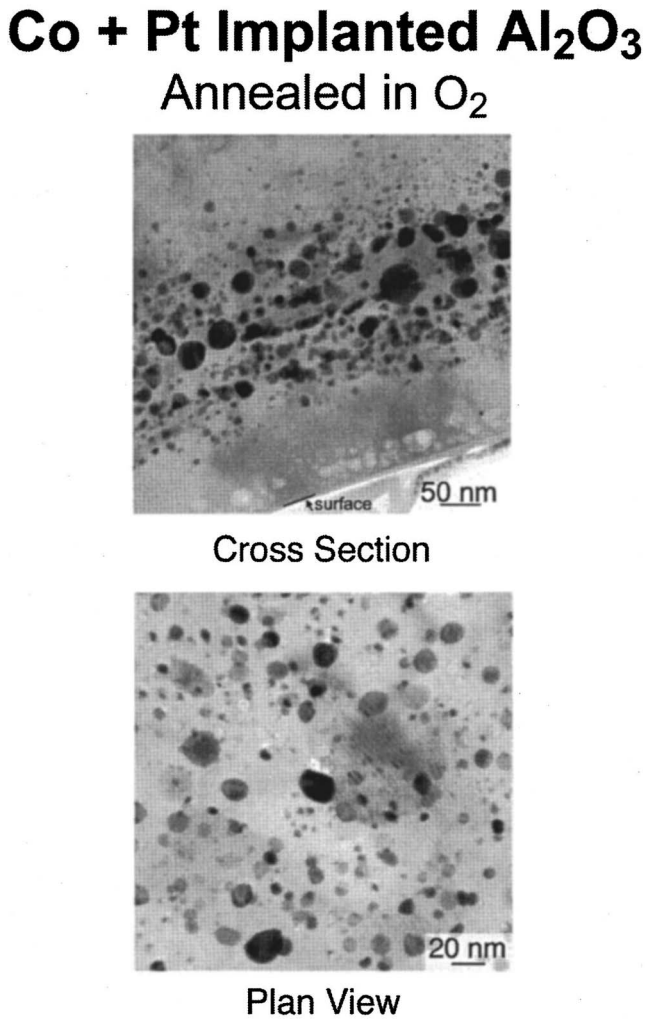

FIG. 3. Cross-section (top) and plan-view (bottom) TEM results for *c*-axis-oriented Al_2O_3 implanted by Co+Pt and annealed in O_2 for 1100 °C/2 h+700 °C/19 h.

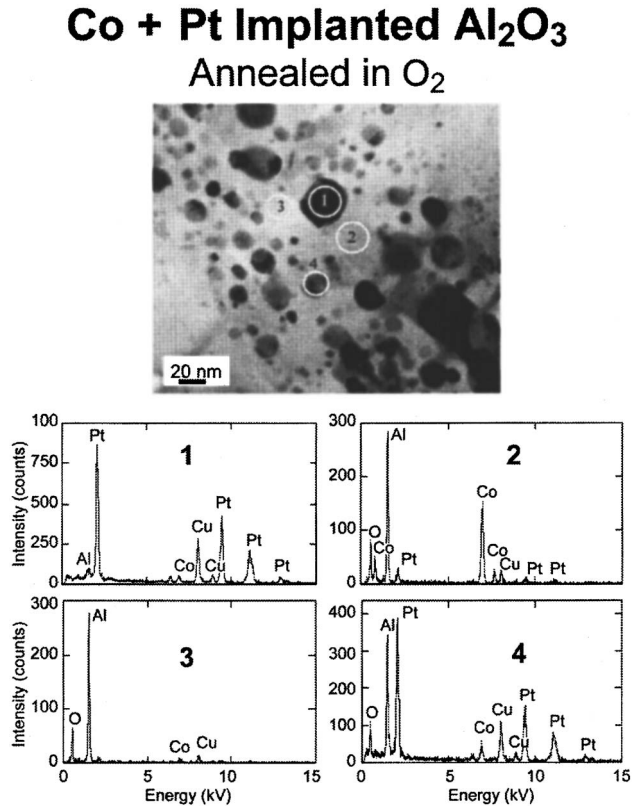

FIG. 4. EDS measurements for Co+Pt implanted Al_2O_3 annealed in O_2 for 1100 °C/2 h+700 °C/19 h. The top shows a portion of the cross-section TEM micrograph taken near the depth of the maximum implanted concentration. The circles with numbers identify regions where the EDS spectra were obtained. The EDS spectra corresponding to these regions are shown below. The x-ray lines arising from individual elements are labeled. The Cu lines arise from the Cu grid in the microscope.

EDS spectra labeled spot 2 is taken from one of these features. This is observed to be Co rich and therefore is most likely the Co_3O_4 nanoparticles identified in the x-ray results in Fig. 1(b). These elongated particles form a layered structure in cross section (and exhibit Moiré fringes in plan view), and this is consistent with the RBS Co profile results of Fig. 2(b). Spot 3 is a region where there are no obvious particles, and the spectra are dominated by lines arising from the matrix. Overall, annealing in O_2 gives rise to Pt rich (approximately pure Pt) and Co rich (Co_3O_4) particles with no evidence of interaction between them.

The magnetic properties of Co+Pt-implanted Al_2O_3 after annealing in ArH_2 or O_2 are compared in Fig. 5. Here, a SQUID magnetometer was used to measure the magnetic moment of the sample (in units of Bohr magnetons per implanted ion) as the applied field was scanned in the range of +65 to −65 kOe. The diamagnetic background signal from the Al_2O_3 substrate has been removed from the data. For the sample annealed in ArH_2 [Fig. 5(a)], the hysteresis in the magnetization data reflects the ferromagnetic nature of the CoPt nanoparticles, which have the chemically ordered fct $L1_0$ structure. The magnetic coercivity of these nanoparticles is high with a value of ~9 kOe at 5 K and ~4.5 kOe at 300 K measured with the field parallel to the surface. (With the field directed along the surface normal, the magnetic coercivities are even higher with values of H_c=13 kOe at 5 K and 6 kOe at 300 K.) The sample annealed in O_2 is dominated by Pt nanoparticles and Co_3O_4 nanoparticles, neither of which is ferromagnetic. (Co_3O_4 is antiferromagnetic with a Néel temperature T_N=33–40 K.[21,22]) Consequently, the magnetization in this sample would be expected to be very low, and this is demonstrated by the data presented in Fig. 5(b) where the magnetic moment is measured to be nearly zero at all field values at 5 and 300 K. On a much more sensitive magnetization scale [Fig. 5(b) inset], there is evidence for residual ferromagnetic behavior at 5 K with a saturation magnetization reduced by a factor of 25 compared with the results obtained by annealing in ArH_2. This suggests that very small quantities of CoPt may be present in this sample, but the concentration is too low to be determined from the x-ray results. Summarizing then, annealing Co+Pt-implanted Al_2O_3 in ArH_2 gives rise to CoPt nanoparticles with the ordered $L1_0$ structure, and these nanoparticles have a high magnetic coercivity and a high saturation magnetization. In contrast, annealing in O_2 results predominately in the precipitation of Pt nanoparticles and Co_3O_4 nanoparticles, with neither being ferromagnetic. The small magnetization after annealing in O_2 may be due to very small quantities of CoPt formed during annealing.

Downloaded 31 Jan 2006 to 160.91.48.40. Redistribution subject to AIP license or copyright, see http://jap.aip.org/jap/copyright.jsp

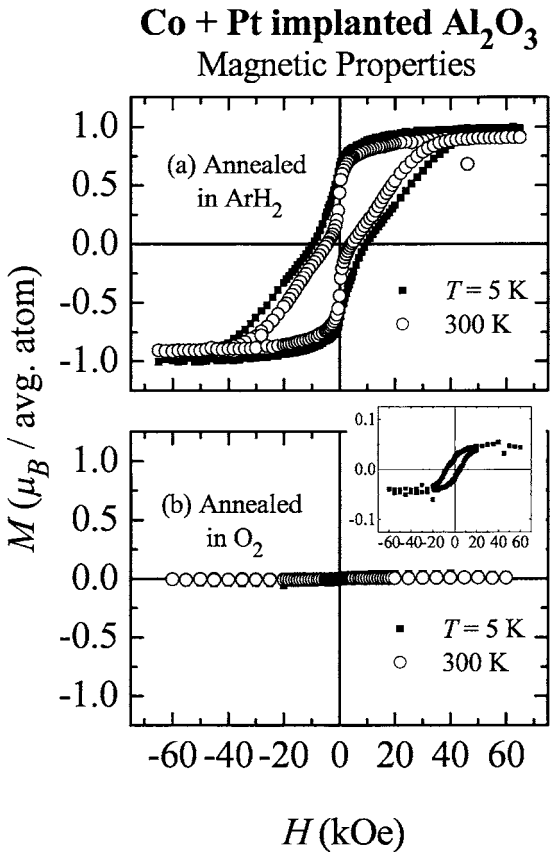

FIG. 5. Magnetization measurements for Co+Pt-implanted Al_2O_3 after annealing in (a) ArH_2 for 1100 °C/2 h+700 °C/119 h and in (b) O_2 for 1100 °C/2 h+700 °C/19 h. The applied magnetic field was parallel to the surface, and measurements were made at T=5 and 300 K. Magnetic moments for the two cases in (a) and (b) are shown on the same vertical scale for ease of comparison. Inset in (b) shows data at T=5 K on a 10× expanded vertical scale.

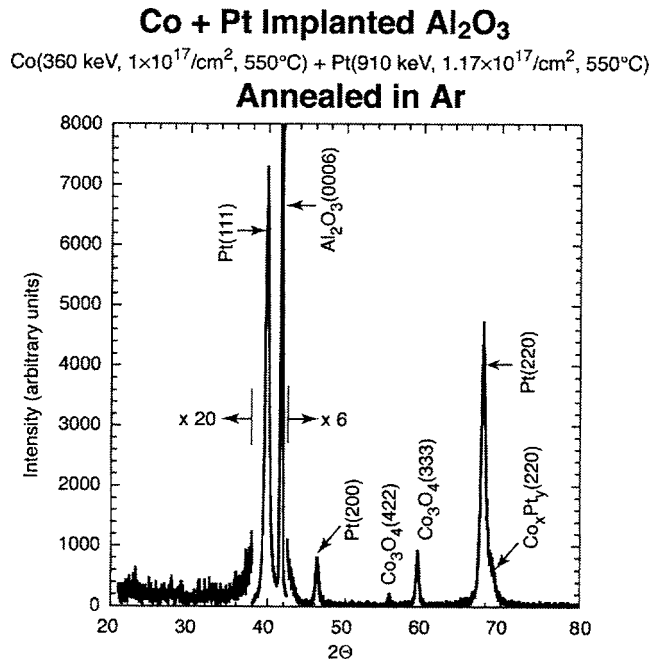

FIG. 6. X-ray-diffraction θ-2θ scans along the surface normal for c-axis-oriented Al_2O_3 implanted by Co+Pt and annealed in Ar (1100 °C/2 h+700 °C/20 h).

Annealing in flowing Ar (99.999% purity) gives results that are nearly the same as those achieved by annealing in O_2. This result is demonstrated by the x-ray-diffraction results in Fig. 6 (on a linear intensity scale), which were obtained using a powder diffractometer. Strong diffraction lines from Pt [Pt (111), Pt (200), and Pt (220)] are observed as well as lines from Co_3O_4 [Co_3O_4(422),Co_3O_4(333)]. The shoulder at $2\theta \sim 69°$ may indicate the presence of small quantities of CoPt nanoparticles, but most of the nanoparticles formed by annealing in Ar are either Pt or Co_3O_4. These results were obtained by annealing in a hot-wall quartz tube furnace with no additional purification of the Ar. These findings are qualitatively consistent with what might be expected from the equilibrium (Ellingham) free-energy diagram[23] for Co in O_2 gas at partial pressures of 10^{-5}–10^{-6} atm at the annealing temperature, where Co_3O_4 (and CoO) are stable with respect to the metal. Accordingly, it is very probable that the oxygen partial pressure in the flowing Ar gas or from the heated quartz provides enough oxygen to dominate the annealing process.

Samples implanted with Co+Pt were also annealed in UHV at pressures of $\sim 5\times 10^{-9}$ or less. These anneals were carried out using a heated sample holder in a chamber with a base vacuum of 5×10^{-11} Torr. The holder with the implanted sample was first degassed at 500 °C for 3 h at a pressure of $\sim 5\times 10^{-10}$ Torr. The holder was then raised to 1100 °C and held there for 2 h. During most of the time at 1100 °C, the chamber pressure was 3×10^{-9} Torr or less (following an initial transient to $\sim 5\times 10^{-9}$ Torr); under these conditions, the oxides of Co are unstable,[23] thereby allowing formation of metallic nanoparticles. After 2 h at 1100 °C, the temperature was reduced to 700 °C and held there for 20 h (pressure of 2×10^{-10} Torr) before cooling to room temperature.

Samples annealed in UHV as described above show evidence for the formation of multiple phases as demonstrated by the x-ray-diffraction results of Fig. 7. Figure 7(a) is a θ-2θ scan along the surface normal and shows multiple strong lines arising from $CoPt_3$. In addition, there is a weak line at $2\theta \sim 59°$ which could arise from either $CoPt_3$ or Co_3O_4. Figure 7(b) is an off-normal scan (i.e., a θ-2θ scan not along the surface normal) showing clear evidence for both $CoPt_3$ lines and for Co_3O_4 lines. The Co_3O_4 nanoparticles probably have incorporated Al as well. We speculate that sluggish kinetics allowed some formation of Co_3O_4 during the second annealing step at 700 °C under which conditions the free energies of the oxide and metal are roughly equal. X-ray rocking curves show that the peaks in Fig. 7(a) represent multiple nanoparticle orientations with respect to the Al_2O_3 matrix, rather than random powder orientations. The diffraction lines labeled as $CoPt_3$ in Fig. 7 are consistent with those expected from the cubic, ordered phase of $CoPt_3$ which has the $L1_2$ structure. Strong lines from a superstructure reflection [$CoPt_3$(110)] as well as the fundamental reflections [$CoPt_3$(111) and $CoPt_3$(220)] are observed. These results demonstrate the formation of $CoPt_3$ nanoparticles with at least some of the particles having the ordered $L1_2$ structure by annealing in UHV. Excess Co, which is not consumed in the formation of $CoPt_3$, appears to precipitate to

Downloaded 31 Jan 2006 to 160.91.48.40. Redistribution subject to AIP license or copyright, see http://jap.aip.org/jap/copyright.jsp

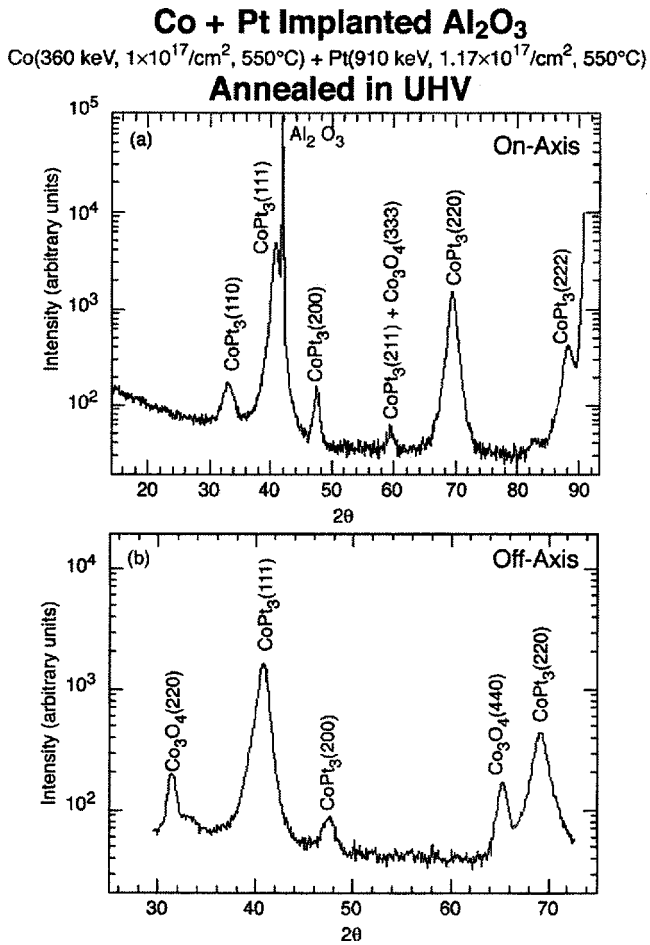

FIG. 7. (a) X-ray-diffraction θ-2θ scans along the surface normal for c-axis-oriented Al_2O_3 implanted by Co+Pt and annealed in UHV for 1100 °C/2 h+700 °C/20 h. (b) Off-normal scan showing both $CoPt_3$ and Co_3O_4 x-ray lines for the sample annealed in UHV.

form Co_3O_4 nanoparticles [from the line identified as the Co_3O_4 (333)reflection in Fig. 7(a) and the Co_3O_4 lines in Fig. 7(b)]. Samples annealed in vacuum at an order of magnitude higher pressure ($\sim 5\times 10^{-8}$ Torr) gave essentially the same results as those in Fig. 7, and showed in addition evidence for Co nanoparticles from a weak line identified as the Co(111) line.

IV. DISCUSSION AND COMPARISON TO RESULTS FOR FE+PT-IMPLANTED AL_2O_3

The results presented here and in our previous work[12] demonstrate that annealing Al_2O_3 implanted with nearly equal doses of Co and Pt (in overlapping profiles) results in the formation of oriented CoPt nanoparticles with the ordered $L1_0$ structure—if the annealing process is carried out in a reducing ArH_2 environment. The order parameter S is estimated to be less than 0.5. The CoPt nanoparticles formed in this manner are ferromagnetic with high coercivities (measured at 5 K) that are in the range of 10 kOe. This coercivity, however, is not as high as others have reported (15–37 kOe) for CoPt films or nanoparticles formed by other methods.[4,9,17,18,24,25] This difference may be related to the smaller degree of ordering achieved in the present work.

These results for Co+Pt-implanted Al_2O_3 annealed in ArH_2 are similar to those for Fe+Pt-implanted Al_2O_3 annealed in the same atmosphere.[13] For Fe+Pt-implanted Al_2O_3, oriented FePt nanoparticles with the chemically ordered $L1_0$ structure are formed during annealing in ArH_2. The nanoparticles can be fully ordered (and probably contain some incorporated Al); they exhibit ferromagnetic behavior, and the magnetic coercivity is extremely high (in excess of 20 kOe) at 5 K.

In contrast, ordered alloy formation does not occur during annealing in O_2 for either Co+Pt- or Fe+Pt-implanted Al_2O_3. In both cases, the implanted Pt precipitates to form oriented Pt nanoparticles, and the implanted Co or Fe reacts with excess O_2 to form oxide nanoparticles or solid solutions with the matrix. However, the oxidation process is different in the two cases. If Co+Pt-implanted Al_2O_3 is annealed in O_2, the oxide precipitate formed is Co_3O_4 that is located in the bulk (i.e., below the surface). For Fe+Pt-implanted Al_2O_3, annealing in O_2 gives rise to segregation of ~40% of the implanted Fe to the surface where it forms oriented Fe_2O_3 surface precipitates.[15] The remainder of the Fe remains in the bulk and forms a solid solution within the matrix. In both cases, there is little or no ordered alloy formation and the magnetic coercivities are very low. The affinity of Pt for oxygen is quite low, so it is not surprising that metallic Pt precipitates are formed during annealing in oxygen. Both Co and Fe will readily react with oxygen, but neither will reduce Al_2O_3. However, if the annealing environment supplies the oxygen, then implanted Co or Fe can readily combine with this oxygen to form oxide precipitates. Others[26] have also found that oxidation must be avoided in order to form ordered FePt nanoparticles by chemical synthesis techniques.

The results obtained by annealing in flowing Ar are very similar to those obtained by annealing in O_2 for either Co+Pt- or Fe+Pt-implanted Al_2O_3. There is little evidence for alloy formation during annealing in Ar for either case. As noted, it is likely that the partial pressure of oxygen in the flowing Ar or from the hot-wall heated quartz furnace provides enough oxygen to dominate the annealing process.

The results obtained by annealing in UHV are considerably different in the two cases. If Co+Pt-implanted Al_2O_3 is annealed in UHV, a mixture of phases is formed including $CoPt_3$, Co_3O_4, and possibly Co, but there is no evidence of CoPt formation from the x-ray results. In contrast, our previous work on Fe+Pt-implanted Al_2O_3 indicated that ordered FePt nanoparticles were formed during annealing in UHV.[15] Thus the FePt material appears to be more stable than CoPt. This observation agrees qualitatively with the respective enthalpies of formation as calculated using the procedure of Miedema and Niessen[27] and Miedema *et al.*[28] In particular, the calculated values for equiatomic compositions are −19.2 kcal/mol of atoms for FePt and −10.6 kcal/mol for CoPt. Hence the enthalpy of formation of the Co-based material is only about one-half of that for the more stable FePt, meaning that CoPt is more susceptible to competition from other phases, as is observed.

Downloaded 31 Jan 2006 to 160.91.48.40. Redistribution subject to AIP license or copyright, see http://jap.aip.org/jap/copyright.jsp

V. CONCLUSIONS

The present work demonstrates that oriented Co_{46} Pt_{54} nanoparticles with the ordered fct $L1_0$ structure are formed by annealing Co+Pt-implanted Al_2O_3 in a reducing atmosphere consisting of 96% Ar+4% H_2. The nanoparticles formed are ferromagnetic and have a magnetic coercivity of ~10 kOe. In contrast, annealing in O_2 (or in 99.999% Ar) gives rise to the precipitation of Pt nanoparticles and the formation of Co_3O_4 oxide nanoparticles with very little evidence for CoPt alloy formation. The magnetization of samples annealed in O_2 is very low. Annealing in UHV results in the formation of a mixture of phases including $CoPt_3$ and Co_3O_4 with no evidence for CoPt. Therefore, the structure and magnetic properties of Co+Pt-implanted Al_2O_3 are strongly dependent on the annealing environment, and in order to form oriented CoPt nanoparticles with hard magnetic properties, it is essential to anneal in a reducing atmosphere, e.g., ArH_2, under conditions similar to those described here.

ACKNOWLEDGMENTS

Research sponsored by the U.S. Department of Energy under Contract No. DE-AC05-00OR22725 with the Oak Ridge National Laboratory, managed by UT-Battelle, LLC.

[1]D. Weller, A. Moser, L. Folks, M. E. Best, W. Lee, M. F. Toney, M. Schwickert, J.-U. Thiele, and M. F. Doerner, IEEE Trans. Magn. **36**, 10 (2000).
[2]M. R. Visokay and R. Sinclair, Appl. Phys. Lett. **66**, 1692 (1995).
[3]M. Yu, Y. Liu, and D. J. Sellmyer, J. Appl. Phys. **87**, 6959 (2000).
[4]J. A. Christodoulides, Y. Huang, Y. Zhang, G. C. Hadjipanayis, I. Panagiotopoulos, and D. Niarchos, J. Appl. Phys. **87**, 6938 (2000).
[5]K. R. Coffey, M. A. Parker, and J. K. Howard, IEEE Trans. Magn. **31**, 2737 (1995).
[6]C.-J. Lin and G. L. Gorman, Appl. Phys. Lett. **61**, 1600 (1992).
[7]G. R. Harp, D. Weller, T. A. Rabedeau, R. F. C. Farrow, and M. F. Toney, Phys. Rev. Lett. **71**, 2493 (1993).
[8]S. Sun, C. B. Murray, D. Weller, L. Folks, and A. Moser, Science **287**, 1989 (2000).
[9]Y. Sui, L. Yue, R. Skomski, X. L. Li, J. Zhou, and D. J. Sellmyer, J. Appl. Phys. **93**, 7571 (2003).
[10]A. Kumbhar, L. Spinu, F. Agnoli, K.-Y. Wang, W. Zhou, and C. J. O'Connor, IEEE Trans. Magn. **37**, 2216 (2001).
[11]N. Yasui, A. Imada, and T. Den, Appl. Phys. Lett. **83**, 3347 (2003).
[12]S. P. Withrow, C. W. White, J. D. Budai, L. A. Boatner, K. D. Sorge, J. R. Thompson, and R. Kalyanaraman, J. Magn. Magn. Mater. **260**, 319 (2003).
[13]C. W. White, S. P. Withrow, K. D. Sorge, A. Meldrum, J. D. Budai, J. R. Thompson, and L. A. Boatner, J. Appl. Phys. **93**, 5656 (2003).
[14]C. W. White, S. P. Withrow, J. D. Budai, L. A. Boatner, K. D. Sorge, J. R. Thompson, K. S. Beaty, and A. Meldrum, Nucl. Instrum. Methods Phys. Res. B **191**, 437 (2002).
[15]C. W. White, S. P. Withrow, J. M. Williams, J. D. Budai, A. Meldrum, K. D. Sorge, J. R. Thompson, and L. A. Boatner, J. Appl. Phys. **95**, 8160 (2004).
[16]*Phase Diagrams: Binary Alloy Phase Diagrams*, edited by T. B. Massalki (American Society of Metals, Metals Park, OH, 1986), Vol. 1, p. 791.
[17]S. H. Liou, Y. Liu, S. S. Malhotra, M. Yu, and D. J. Sellmyer, J. Appl. Phys. **79**, 5060 (1996).
[18]R. A. Ristau, K. Barmak, L. H. Lewis, K. R. Coffey, and J. K. Howard, J. Appl. Phys. **86**, 4527 (1999).
[19]JCPDS-International Center for Diffraction Data, Card No. 43-1358, 2000.
[20]B. E. Warren, *X-Ray Diffraction* (Addison-Wesley, Reading, MA 1969), Chap. 12.
[21]W. L. Roth, J. Phys. Chem. Solids **25**, 1 (1964).
[22]W. Kundig, M. Kobelt, H. Appel, G. Constabaris, and R. H. Lindquist, J. Phys. Chem. Solids **30**, 819 (1969).
[23]T. B. Reed, *Free Energy of Formation of Binary Compounds* (MIT, Cambridge, MA, 1971).
[24]S. H. Liou, S. Huang, E. Klimek, R. D. Kirby, and Y. D. Yao, J. Appl. Phys. **85**, 4334 (1999).
[25]S. Stavroyiannis, I. Panagiotopoulos, D. Niarchos, J. A. Christodoulides, Y. Zhang, and G. C. Hadjipanayis, J. Magn. Magn. Mater. **193**, 181 (1999).
[26]C. Liu, T. J. Klemmer, N. Shukla, X. Wu, D. Weller, M. Tanase, and D. Laughlin, J. Magn. Magn. Mater. **266**, 96 (2003).
[27]A. R. Miedema and A. K. Niessen, CALPHAD: Comput. Coupling Phase Diagrams Thermochem. **7**, 27 (1983).
[28]A. R. Miedema, F. R. deBoer, and R. Boom, CALPHAD: Comput. Coupling Phase Diagrams Thermochem. **1**, 341 (1977).

Downloaded 31 Jan 2006 to 160.91.48.40. Redistribution subject to AIP license or copyright, see http://jap.aip.org/jap/copyright.jsp